INVERSION OF SNOW STRUCTURE PARAMETERS FROM TIME SERIES OF TOMOGRAPHIC MEASUREMENTS WITH SNOWSCAT

Othmar Frey
Gamma Remote Sensing /
Earth Observation & Remote Sensing, ETH Zurich
Switzerland
Email: frey@gamma-rs.ch

Charles L. Werner, Rafael Caduff, Andreas Wiesmann
Gamma Remote Sensing
Switzerland
Email: {cw, caduff, wiesmann}@gamma-rs.ch

***Abstract*—SnowScat is a terrestrial stepped-frequency continuous-wave (SFCW) scatterometer which supports fully-polarimetric measurements within a frequency band from 9.2 to 17.8 GHz. Recently, the hardware has been upgraded by adding a tomographic profiling mode. This tomographic approach allows to retrieve high-resolution information about a snowpack via observables, such as radar backscatter, co-polar phase difference, interferometric phase and coherence. Since the tomographic imaging itself is also affected by the refraction occurring at the air-snow interface and within the snowpack the two problems, 1) the production of well-focused and correctly located tomographic profiles, and 2) the retrieval of snow structure parameters are inherently linked. In this contribution, a tomographic inversion scheme to retrieve the refractive index of snow through an autofocus approach is presented. The current autofocus-based retrieval relies on using an aluminium sphere of a test target deployed in the scene. The refractive indices and accompanying snow density measurements obtained at four dates during a cold period in January during the ESA SnowLab 2016/2017 campaign are compared to an empirical model by Matzler and Wiesmann that describes the relation between snow density and the real part of the relative permittivity for dry snow.**

***Index Terms*—SnowScat, microwave remote sensing, snow, tomography, tomographic profiling, SAR tomography, scatterometer, time series, X-band, Ku-band, European Space Agency, ESA.**

I. Introduction

SnowScat is a terrestrial stepped-frequency continuous-wave (SFCW) scatterometer which supports fully-polarimetric measurements within a frequency band from 9.2 to 17.8 GHz [1] [2]. Designed originally to support the investigation and validation of snow water equivalent (SWE) retrieval algorithms, see e.g. [3], in the context of the CoReH20 candidate Earth Explorer 7 mission the SnowScat hardware has meanwhile been enhanced by adding a tomographic profiling mode. Using the SnowScat device in tomographic profiling mode, it is possible to non-destructively retrieve high-resolution information on the spatial variation of radar backscatter, co-polar phase difference, interferometric phase and coherence; observables that may vary with spatially and temporally changing properties of the snowpack.

In winter 2014/2015, a first test campaign at a test site hosted by the WSL Institute for Snow and Avalanche Research (SLF), in Davos, Switzerland was carried out yielding a successful proof of concept of the enhanced hardware, the tomographic measurement, and a basic processing concept.

TABLE I
System specifications of the SnowScat device in tomographic profiling mode during the ESA SnowLab experiment at the testsite Davos Laret, winter 2016/2017

Frequency	SFCW from 9.2 to 17.8GHz
Nominal incidence angle	45^o
Sampling spacing	0.04 m
Number of samples	50
Synth. aperture length	1.96 m
3dB res. (stripmap m.)	0.15 m
Polarization	HH, HV, VV, VH
Dynamic range	Receiver dynamic range $>$ 80dB with the 16bit ADC
Signal bias	$<$ 0.5dB
Gain characterization	Internal calibration, calibration sphere (Ø = 254mm)
RFI	Frequency blacklist

First comparisons of tomographic profiles with in-situ snow profiles indicated that melt-freeze crusts/ice layers present within the snowpack could be identified [4] [5]. This is in accordance with similar findings reported in [6] [7] [8] [9]. In [10], first results of a time series of tomographic profiles including 2-D vertical profiles of backscatter, phase difference between the co-polar channels, and interferometric phase difference were presented.

Obviously, the tomographic imaging of the snowpack itself is also affected by the refraction occurring at the air-snow boundary surface and within the snowpack. Therefore, the two problems, 1) generating well-focused and correctly located tomographic profiles, and 2) retrieving snow structure parameters from the tomographic measurements, are closely linked and must be solved simultaneously, at least considering the refraction. In this contribution, a tomographic inversion and parameter retrieval scheme for the refractive index is discussed. It takes advantage of the effect that (previously unknown) refraction has on SAR image focusing through an autofocus approach. The current autofocus-based retrieval relies on using an aluminium sphere of a test target deployed in the scene. The refractive indices and accompanying snow density measurements obtained at four dates during a cold period in January during the latest ESA SnowLab 2016/2017 campaign are compared to an empirical model that describes the relation between snow density and the real part of the relative permittivity for dry snow.

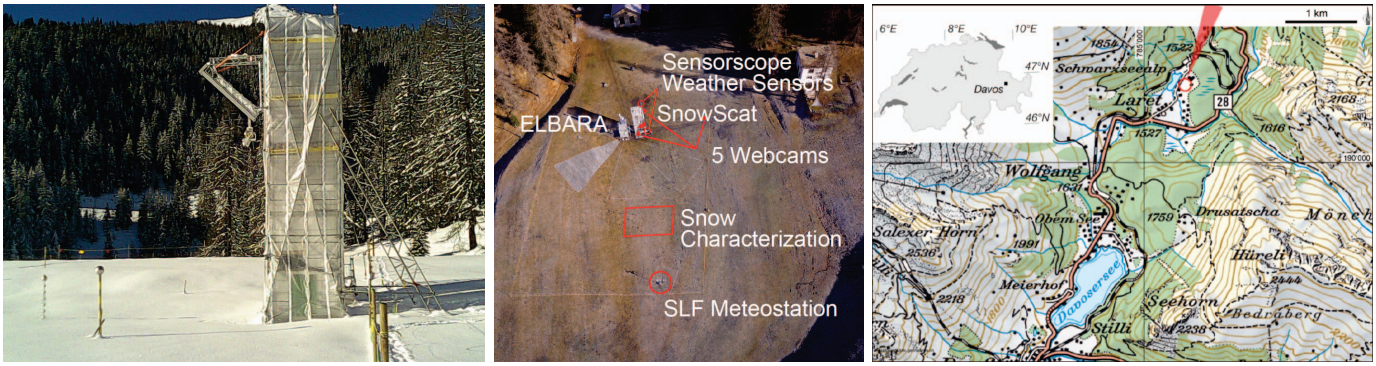

(a) (b) (c)

Fig. 1. a) The SnowScat device, movable on a rail for tomographic data acquisitions, during the ESA Snowlab campaign at the test site Davos Laret, Switzerland, snow season 2016/2017. On the left, the tomographic test target, a vertical array of eight aluminium spheres mounted on a carbon rod, and a calibration sphere are visible. b) Aerial view of the test site indicating the location of the various sensors deployed during the campaign and the location of the field for *in-situ* snow characterisation (UAS image by Y. Bühler and M. Jaggi, SLF). c) Map overview of the test site.

II. Test Site and Experimental Data

A. ESA SnowLab experimental setup 2016/2017

In winter 2016/2017, the SnowScat device was operated in the Swiss Alps at a new test site in Davos Laret (approx. 1500 m a.s.l.) hosted by the WSL Institute for Snow and Avalanche Research (SLF). In Fig. 1 an overview of the test site is given. During the entire snow season a tomographic profile was acquired per day. A tomographic acquisition consists of moving the SnowScat device along a rail and taking 50 measurements at intervals of 4cm. For further details on the tomographic measurement setup see Table I and [4], [5]. The SnowScat measurements were accompanied by repeated *in-situ* snow characterisations, meteorological sensor measurements and five webcams. In Fig. 2, a plot of *in-situ* snow density measurements is shown. The snow density measurements are used to assess the tomography-based retrieval of the relative permittivity.

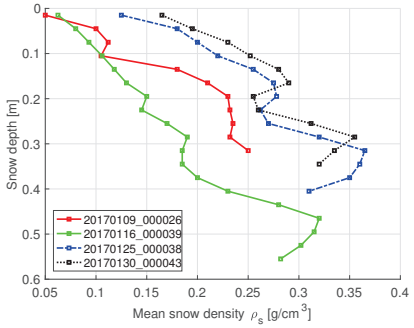

Fig. 2. *In-situ* snow density measurements taken within the designated snow characterisation field at the Davos Laret test site at four days 2017-01-09, 2017-01-16, 2017-01-25, and 2017-01-30. The snow density profiles were measured by a density cutter with a vertical resolution of 3 cm.

III. Methods

A. SnowScat tomography and autofocus-based retrieval

The basis for the tomographic inversion of the snowpack is a time-domain back-projection (TDBP)-based approach [11], [12]. The advantage of the TDBP approach is its ray-tracing-like calculation of the wave propagation through the inhomogeneous media. A virtual range distance R_v can be calculated iteratively based on the incidence angle θ, the angle of refraction θ_S, the refractive index n_s, and the different phase velocities c (in air) and v_S (in the snow volume). The delay-and-sum approach of the TDBP focusing reads (omitting the antenna gain pattern and the range-spreading loss):

$$v(\mathbf{r}_i, n_s) = \sum_{k=1}^{M} g_k[R_v(\mathbf{r}_i, \mathbf{r}_k, n_s)] \cdot \exp[i\, 4\pi/\lambda R_v(\mathbf{r}_i, \mathbf{r}_k, n_s)] \; . \tag{1}$$

where $\mathbf{r}_i$ is the 3-D position vector of the target location at which the tomographic inversion is calculated, $\mathbf{r}_k$ is the 3-D position vector of the antenna phase centre at position k within the synthetic aperture. $g_k(...)$ is the range-compressed signal at antenna position k, λ is the wavelength of the carrier signal, and $R_v(\mathbf{r}_i, \mathbf{r}_k, n_s)$ is the (virtual) range distance between antenna position k and the location $\mathbf{r}_i$ taking into account the refraction within a snow layer, assumed to be homogenous.

The calculation of the point of entry at the air/snow interface is based on the trigonometric relationships as depicted in Fig. 3, reproduced from [13]. The virtual range distance R_v can be expressed as follows (using the terms from Fig. 3):

$$R_v = n_a \sqrt{d_{a/s}^2 + d_a^2} + n_s \sqrt{(d_p - d_{a/s})^2 + d_s^2}. \tag{2}$$

$v(\mathbf{r}_i, n_s)$ is the focused signal at location $\mathbf{r}_i$. Essentially the refractive index n_s is then retrieved by maximising the averaged intensity $\langle \hat{I} \rangle = \langle |v(\mathbf{r}_i, n_s)|^2 \rangle$:

$$\hat{n}_s = \underset{n_s \in \mathbb{N}_s}{\arg\max} \left(\langle \hat{I} \rangle \right) \; . \tag{3}$$

The basic idea behind the autofocus-based retrieval is that the relative intensity (or another suitable function) reaches a maximum in the case where the refractive index, as a parameter of the virtual range distance, matches the physical properties of the snowpack. The current approach is based on

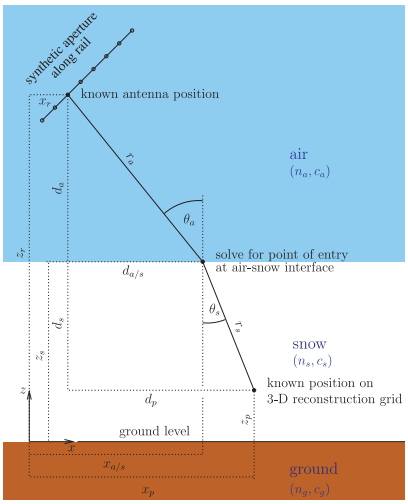

Fig. 3. Sketch of simplified acquisition scenario for tomographic profiling of a snowpack with the SnowScat device as shown in [13].

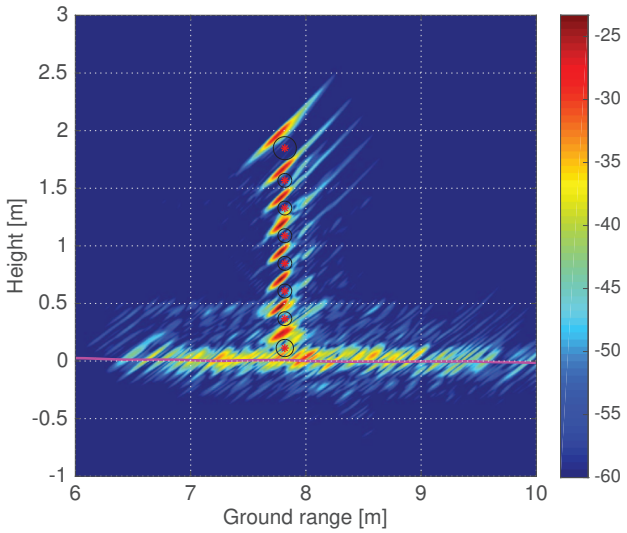

Fig. 4. Tomographic profile (VV channel, rel. intensity) produced from the data take 2017-01-25 after running the autofocus retrieval. The nominal position and shape of the tomographic test target are also indicated in the plot. The local terrain height as obtained from close-range digital photogrammetry is plotted as a magenta-coloured line.

a number of simplifying assumptions: A homogenous one-layer snowpack and therefore a constant snow density are assumed. The *in-situ* measurements of snow density profiles clearly show a different behaviour with a considerable vertical variation of the snow density for each of the four dates. In addition, the snow height is an input variable for the autofocus-based inversion. It can be retrieved from averaging the snow profiles along ground range, though.

B. Refractive index, relative permittivity and snow density

The complex dielectric constant $\epsilon = \epsilon' + i\epsilon''$ and the complex refractive index $N = n' + in''$ are related through $N = \sqrt{\epsilon}$ [14]. The real part ϵ' of the complex dielectric constant is the relative permittivity (also: real part of the relative permittivity), the imaginary part ϵ'' is a loss factor. The real part n' of the complex refractive index N is linked to the propagation velocity of the electromagnetic wave in the medium, and is thus the parameter of interest in terms of the autofocus-based retrieval. It is then converted to the (real part of the) relative permittivity $\epsilon' = n'^2 - n''^2$, where the term n''^2 can be neglected for dry snow and microwave frequencies operated by SnowScat [14] and $n' = n_s$ in accordance with our previous notation. For dry snow and within the range of frequencies that are transmitted by the SnowScat device the relative permittivity ϵ' was shown to be related to snow density [15], [16]. The model relating snow density ρ_s and the relative permittivity ϵ' for dry snow and the range of values of snow densities relevant here is: [15]:

$$\epsilon' = 1 + 1.5995\rho_s + 1.861\rho_s^3, 0 < \rho_s < 0.4g/cm^3 \ . \quad (4)$$

IV. Results

By means of the tomographic inversion approach (an example of a tomographic profile is given in Fig. 4) a relative permittivity is retrieved under the assumption that the snowpack is homogeneous. To this end, the relative backscattering intensity is maximised. Fig. 5a) explicitly shows the function that is relevant for the retrieval: the average relative backscattering intensity within a window around the specular reflection point of the lower-most sphere of the tomographic test target. The function is shown for those four dates where also accompanying *in-situ* snow density measurements are available. All curves show a clear absolute maximum leading to an unambiguous estimate of the relative permittivity.

In Fig. 5b) the relative permittivities found by autofocus from SnowScat tomography data are plotted against an average snow density, which is obtained from averaging the *in-situ* snow density profiles above the vertical position of the test sphere. The model by Wiesmann and Matzler [15], [16], relating snow density and relative permittivity for dry snow, is also plotted, coloured in magenta, and flanked by 5% intervals given in dashed lines.

V. Discussion

A comparison of the relative permittivities retrieved from the SnowScat tomographic profiles and of the measured snow densities with the model by [15] given in eq. (4) indicates that the trend of the model is well represented by the data pairs.

As can be seen from the snow density profiles measured *in situ* (cf. Fig. 2) the snow density varies considerably with the vertical axis. This variation in snow density is present although the snow cover is still relatively homogeneous without any pronounced layering structure (e.g. melt-freeze crusts) visible in the backscattering image. The soil was frozen before the first snowfall and also the air temperature remained below 0^oC during the entire measurement cycle in January 2017. The fine spatial scale of the snow density variation is certainly challenging for any retrieval approach and is presumably

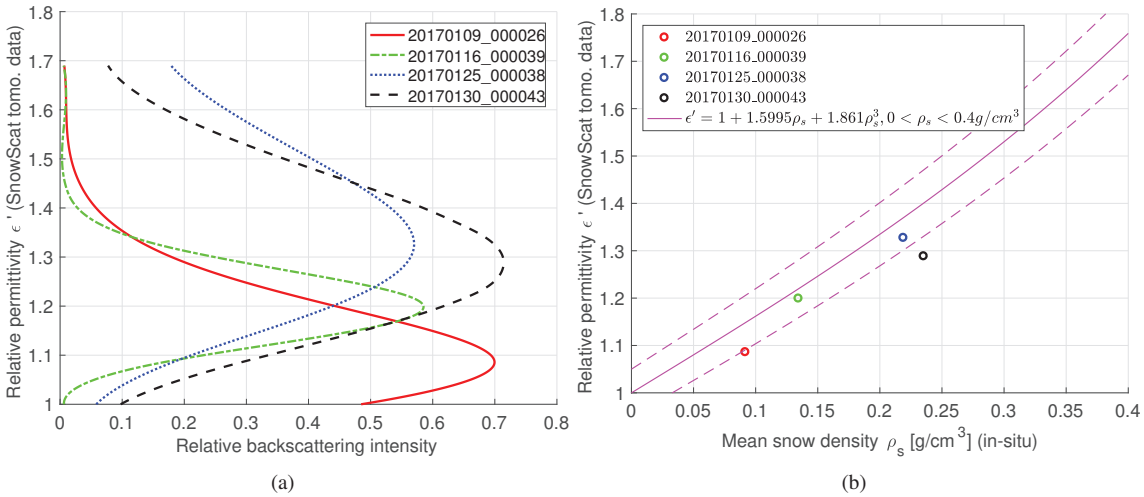

(a) (b)

Fig. 5. a) The function maximised in the autofocus procedure, namely the average relative backscattering intensity within a window around the specular reflection point of the lower-most sphere of the tomographic test target, is reproduced here explicitly for varying relative permittivities (or refractive indices) and for four dates 2017-01-09, 2017-01-16, 2017-01-25, and 2017-01-30, at which *in-situ* snow density measurements are available. All curves show a clear absolute maximum. b) Plot of the relative permittivities retrieved by autofocus from SnowScat tomography data versus the mean snow density as obtained from averaging the snow density profile above the location of the test sphere. Colored in magenta, and flanked by 5% intervals given in dashed lines, an empirical model by Wiesmann and Matzler [15], [16] is plotted. The model describes the relation between snow density and relative permittivity for dry snow.

one of the factors that lead to a slight underestimation of the relative permittivity compared to the empirical model by Wiesmann and Matzler [15], [16].

Another potential source for remaining differences between the model and measured data is the fact that time and location of the data acquisition of SnowScat measurement and the snow density cutter measurements do not coincide: the tomographic profiling with SnowScat takes place in the first hours of the day whereas the in-situ measurements were taken throughout the day. Besides potentially different snow densities at the two locations, particularly, a mismatch in the snow depth can also be of relevance since the depth is an external parameter fed into the autofocus scheme (either extracted from the averaged vertical profile itself or given externally). Bearing these limitation factors in mind, the measured and retrieved parameters are found to be in good agreement with the empirical model.

Acknowledgment

The ESA SnowLab campaign has been conducted in the frame of ESA/ESTEC Contract No. 4000117123/16/NL/FF/MG. M. Schneebeli and M. Jaggi, WSL Institute for Snow and Avalanche Research (SLF), are gratefully acknowledged for the *in situ* measurements.

References

[1] A. Wiesmann, C. L. Werner, C. Matzler, M. Schneebeli, T. Strozzi, and U. Wegmuller, "Mobile X- to Ku-band scatterometer in support of the CoRe-H2O mission," in *Proc. IEEE Int. Geosci. Remote Sens. Symp.*, vol. 5, July 2008, pp. 244–247.

[2] C. L. Werner, A. Wiesmann, T. Strozzi, M. Schneebeli, and C. Matzler, "The SnowScat ground-based polarimetric scatterometer: Calibration and initial measurements from Davos Switzerland," in *Proc. IEEE Int. Geosci. Remote Sens. Symp.*, July 2010, pp. 2363–2366.

[3] S. Leinss, A. Wiesmann, J. Lemmetyinen, and I. Hajnsek, "Snow water equivalent of dry snow measured by differential interferometry," *IEEE Journal of Selected Topics in Applied Earth Observations and Remote Sensing*, vol. 8, no. 8, pp. 3773–3790, Aug 2015.

[4] O. Frey, C. L. Werner, M. Schneebeli, A. Macfarlane, and A. Wiesmann, "Enhancement of SnowScat for tomographic observation capabilities," in *Proc. FRINGE 2015*, ser. ESA SP-731, Mar. 2015.

[5] O. Frey, C. L. Werner, and A. Wiesmann, "Tomographic profiling of the structure of a snow pack at X-/Ku-band using SnowScat in SAR mode," in *Proc. EuRAD 2015 - 12th European Radar Conference*, Sept. 2015, pp. 21–24.

[6] S. Tebaldini and L. Ferro-Famil, "High resolution three-dimensional imaging of a snowpack from ground-based SAR data acquired at X and Ku band," in *Proc. IEEE Int. Geosci. Remote Sens. Symp.*, July 2013, pp. 77–80.

[7] L. Ferro-Famil, S. Tebaldini, M. Davy, and F. Boute, "3D SAR imaging of the snowpack at X- and Ku-band: results from the AlpSAR campaign," in *Proc. of EUSAR 2014 - 10th European Conference on Synthetic Aperture Radar*, June 2014, pp. 1–4.

[8] K. Morrison and J. Bennett, "Tomographic profiling - a technique for multi-incidence-angle retrieval of the vertical SAR backscattering profiles of biogeophysical targets," *IEEE Trans. Geosci. Remote Sens.*, vol. 52, no. 2, pp. 1350–1355, Feb. 2014.

[9] B. Rekioua, M. Davy, and L. Ferro-Famil, "Snowpack characterization using SAR tomography: experimental results of the AlpSAR campaign," in *Radar Conference (EuRAD), 2015 European*, Sept 2015, pp. 33–36.

[10] O. Frey, C. L. Werner, R. Caduff, and A. Wiesmann, "A time series of tomographic profiles of a snow pack measured with snowscat at x-/ku-band," in *Proc. IEEE Int. Geosci. Remote Sens. Symp.*, vol. 1, July 2016, pp. 17–20.

[11] O. Frey, F. Morsdorf, and E. Meier, "Tomographic imaging of a forested area by airborne multi-baseline P-band SAR," *Sensors, Special Issue on Synthetic Aperture Radar*, vol. 8, no. 9, pp. 5884–5896, Sept. 2008.

[12] O. Frey and E. Meier, "3-D time-domain SAR imaging of a forest using airborne multibaseline data at L- and P-bands," *IEEE Trans. Geosci. Remote Sens.*, vol. 49, no. 10, pp. 3660–3664, Oct. 2011.

[13] O. Frey, C. L. Werner, R. Caduff, and A. Wiesmann, "A time series of SAR tomographic profiles of a snowpack," in *Proc. of EUSAR 2016 - 11th European Conference on Synthetic Aperture Radar*, June 2016, pp. 726–730.

[14] M. N. O. Sadiku, "Refractive index of snow at microwave frequencies," *Appl. Opt.*, vol. 24, no. 4, pp. 572–575, Feb. 1985.

[15] A. Wiesmann and C. Matzler, "Microwave emission model of layered snowpacks," *Remote Sensing of Environment*, vol. 70, no. 3, pp. 307–316, 1999.

[16] C. Matzler, "Microwave permittivity of dry snow," *IEEE Transactions on Geoscience and Remote Sensing*, vol. 34, no. 2, pp. 573–581, 1996.